Surface and Interface Studies of GaN Epitaxy on Si(111) via ZrB_2 Buffer Layers

Yukiko Yamada-Takamura,[1] Z. T. Wang,[1] Y. Fujikawa,[1] T. Sakurai,[1] Q. K. Xue,[1,*] J. Tolle,[2] P.-L. Liu,[3] A. V. G. Chizmeshya,[4] J. Kouvetakis,[2] and I. S. T. Tsong[3]

[1]*Institute for Materials Research, Tohoku University, Sendai 980-8577, Japan*
[2]*Department of Chemistry and Biochemistry, Arizona State University, Tempe, Arizona 85287-1604, USA*
[3]*Department of Physics and Astronomy, Arizona State University, Tempe, Arizona 85287-1504, USA*
[4]*Center for Solid State Science, Arizona State University, Tempe, Arizona 85287-1704, USA*

(Received 13 July 2005; published 28 December 2005)

Gallium nitride films, epitaxially grown on Si(111) via a lattice-matched ZrB_2 buffer layer by plasma-assisted molecular beam epitaxy, have been studied *in situ* by noncontact atomic force microscopy and also in real time by reflection high-energy electron diffraction. The grown films were determined to be always N-polar. First-principles theoretical calculations modeling the interface structure between GaN(0001) and ZrB_2(0001) clarify the origin of the N polarity.

DOI: 10.1103/PhysRevLett.95.266105 PACS numbers: 68.35.Ct, 68.37.Ps, 81.05.Ea

Gallium nitride-based optoelectronics devices grown on sapphire and SiC now dominate blue as well as white light-emitting diodes and blue laser diode production [1]. Recently, the interest in growing GaN on Si substrates has been revived [2] due partly to the desire to seek a lower-cost alternative to the conventional substrates and partly to the potential capability of integrating high-power high-frequency nitride electronics with silicon integrated circuits. However, serious problems remain because of the large lattice mismatch and thermal expansion mismatch between GaN and Si. Silicon also absorbs visible and UV light, in contrast with sapphire and SiC [3], thereby reducing the light output from the active light-emitting nitride layers. Aluminum nitride and other nitride buffer layers have been successfully employed to grow III-nitride layers on Si(111) with a high degree of quality, but they still suffer from low external quantum efficiencies arising from the absorption losses in the substrate [2]. Distributed Bragg reflectors which consist of multiple $Al_xGa_{1-x}N$ stacking layers are designed to avoid the losses [4], but they have to be tuned for a range of desired wavelengths by tailoring the absorption coefficients of the layers. A suitable metallic buffer layer on Si which solves all these problems will be highly desirable. Single crystals of ZrB_2 [5], a semimetal with AlB_2-type hexagonal structure and an in-plane lattice constant $a = 3.168$ Å closely matching that of 3.189 Å for GaN, have been demonstrated recently to be viable substrates for III nitrides [6]. We have succeeded in growing ZrB_2(0001) epitaxially on Si(111) and used it to grow III-nitride films which exhibit promising photoluminescence properties [7–9]. However, the fundamental question on the interface structure between GaN and ZrB_2, which in turn determines the polarity of the GaN film, remains open. The chemical and physical properties of GaN films are known to be strongly dependent on their polarity [10]. The determination of the interface structure and the polarity of GaN films grown on Si(111) via ZrB_2 buffer layers is, therefore, not only of scientific interest but also of technological significance.

In this Letter, we show that atomically flat and monopolar GaN films can be readily grown on Si(111) by using clean ZrB_2(0001) buffer layers. Under optimized growth conditions, the GaN films always exhibit the single N polarity, as demonstrated by combined *in situ* reflection high-energy electron diffraction (RHEED) and noncontact atomic force microscopy (NC-AFM) studies. Our experimental results are further supported by first-principles theoretical calculations of the stable interface structures.

The ZrB_2(0001) films, with a thickness of 15 nm, were grown on Si(111) at Arizona State University using the method described in Refs. [7–9]. The samples were delivered to Tohoku University, then cut, cleaned ultrasonically with acetone and ethanol, rinsed in deionized water, and installed in our ultrahigh vacuum (UHV) molecular beam epitaxy (MBE)–scanning probe microscopy–x-ray photoelectron spectroscopy (XPS) system [11]. The base pressure of the system is better than 1×10^{-8} Pa.

In contrast with the high temperature and complex procedure for cleaning the bulk ZrB_2 crystal surfaces [12], we find that the ZrB_2 films could be cleaned by simple direct current heating at 750–800 °C under UHV. The as-loaded sample showed carbon (not shown), Zr-O, and B-O related peaks in addition to ZrB_2 related peaks in XPS spectra measured with Al $K\alpha$ radiation as shown in Fig. 1(a). The C 1*s* peak disappeared after heating the sample to temperatures ≤ 750 °C. The oxide-related peaks disappeared when heated to ≥ 750 °C overnight as shown in Fig. 1(a). The oxide-free ZrB_2 film surface showed a streaky ZrB_2(0001)-(2×2) RHEED pattern at RT as shown in Fig. 1(b). The atomically smooth surface with the reconstructed (2×2) surface was also observed by scanning tunneling microscopy (STM) as shown in Figs. 1(c) and 1(d). The average width of the terraces was about 50 nm,

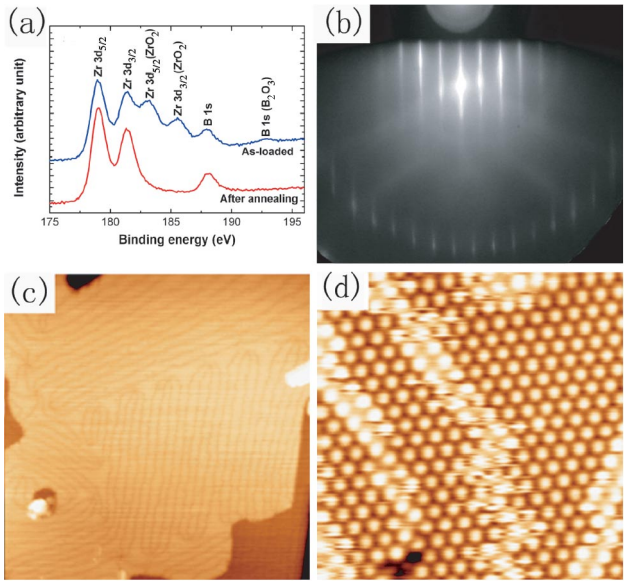

FIG. 1 (color). (a) XPS spectra of as-loaded ZrB_2 film (blue) and annealed film (red) in B 1*s* and Zr 3*d* regions. Oxide-related peaks disappeared after annealing at 760 °C overnight under UHV. (b) RHEED pattern of oxide-free $ZrB_2(0001)$ film showing 2× streaks at RT. The electron beam is parallel to $ZrB_2\langle 11\bar{2}0\rangle$. STM images of the $ZrB_2(0001)$-(2×2) surface (c) 100×100 nm^2 (+0.9 V, 0.15 nA), showing terraces with narrow antiphase domains and step heights of about 0.34 nm, similar to the *c* lattice constant of ZrB_2, and (d) 10×10 nm^2 (+0.1 V, 1.5 nA), showing atomically resolved (2×2) reconstruction with antiphase domain boundaries in brighter contrast.

and domains with typical widths of a few nanometers were observed. The step height between the neighboring terraces is 0.34 ± 0.02 nm, identical to the *c* lattice constant of 0.353 nm, indicating that the surface is terminated by either a Zr layer or a B_2 layer. The thermally treated single crystal ZrB_2 surface was determined to be Zr-terminated [12], but the termination of our film is an open question.

The epitaxial growth of GaN films was conducted on the $ZrB_2(0001)$-(1×1) surface at temperatures of 700 ± 30 °C, after the original (2×2) reconstruction underwent a reversible transition to (1×1). The Ga cell temperature was set to about 1000 °C to achieve optimal growth condition, i.e., a slightly Ga-rich condition [11], and the rf plasma source was operated at 300 W power with a N_2 pressure of 3×10^{-3} Pa. The GaN surface was monitored by RHEED, which changed from the streaky $ZrB_2(0001)$-(1×1) pattern to a spotty hexagonal GaN(0001) pattern, and finally to a streaky GaN(0001)-(1×1) pattern, demonstrating the atomically smooth GaN growth. Based on the peak separations and rotation symmetry, it was determined that the epitaxial relationship between GaN and ZrB_2 follows $GaN\langle 0001\rangle \parallel ZrB_2\langle 0001\rangle$ and $GaN\langle 11\bar{2}0\rangle \parallel ZrB_2\langle 11\bar{2}0\rangle$, reflecting their near-perfect in-plane lattice matching.

Deposition of Ga on the GaN(0001)-(1×1) surface at RT resulted in (3×3), (6×6), and $c(6\times 12)$ RHEED patterns with increasing Ga coverage. It turned out that STM imaging of these reconstructed surfaces was impossible because of the insulating nature of the film. Previously, we have demonstrated that STM imaging was easily achieved on surfaces of GaN films grown directly on Si(111) [11], where the GaN was likely doped *n*-type unintentionally by Si. However, in the present case, the ZrB_2 buffer layer was an effective diffusion barrier against Si doping of the GaN films from the substrate, consistent with our previous high-mass-resolution secondary ion mass spectrometry measurement [9]. In order to study the detailed atomic structure of the insulating intrinsic GaN surface, it was necessary to use NC-AFM. A Si cantilever with reflective metal coating with a resonance frequency of about 300 kHz and a force constant of typically 50 N/m was used under constant excitation voltage. The images were observed in constant frequency shift (Δf) mode, and the atomic resolution was achieved at Δf between -60 and -90 Hz. No bias voltage was applied to the sample. Figure 2(a) shows an AFM image of the atomically smooth GaN surface, where a screw dislocation is observed. All Ga-rich $GaN(000\bar{1})$ reconstructions, (3×3), (6×6), and $c(6\times 12)$ [13], were observed in atomic resolution, as shown in Figs. 2(b)–2(d), respectively. The AFM images were remarkably similar to the STM images observed in Ref. [13], thus leading to the identification of N polarity of the GaN film grown on $ZrB_2(0001)/Si(111)$.

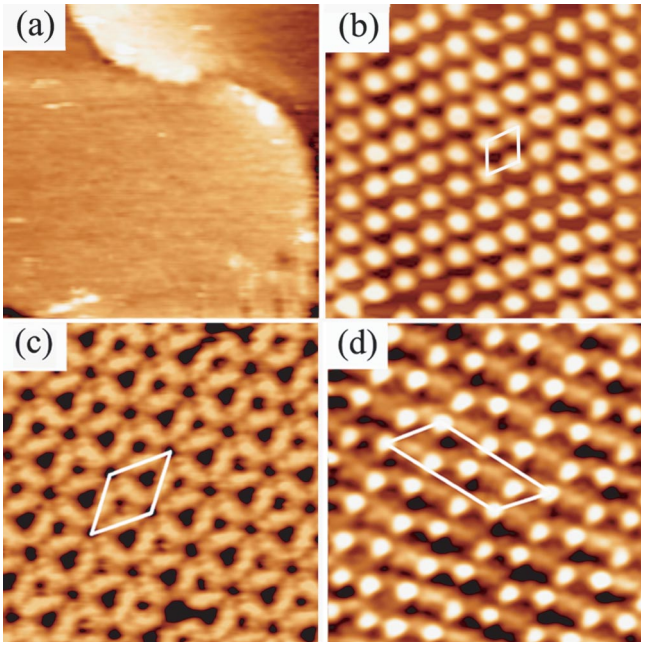

FIG. 2 (color). NC-AFM images of a GaN film surface grown on $ZrB_2/Si(111)$. (a) Scan size 100×100 nm^2, showing part of a spiral dislocation structure on an atomically flat $GaN(000\bar{1})$ surface. Scan size 10×10 nm^2, showing (b) (3×3), (c) (6×6), and (d) $c(6\times 12)$ reconstructions. (b), (c), and (d) are surface reconstructions all related to the N-polar $GaN(000\bar{1})$ surface.

Smith *et al.* [13] studied the bias voltage dependence of the STM images for each of these Ga-rich GaN(000$\bar{1}$) reconstructions and observed strong dependence only for the $c(6 \times 12)$ structure. We note that the AFM image of the $c(6 \times 12)$ structure, shown in Fig. 2(d), is nearly identical to the empty state STM image rather than the filled state image reported in Ref. [13] and in our previous study [11]. Since optimization to achieve atomic resolution was done by gradually increasing Δf, i.e., decreasing the probe-sample distance, the probe must have interacted with the empty state spreading outside the filled state of $c(6 \times 12)$ structure, giving an AFM image identical to the empty state STM image. Since the $c(6 \times 12)$ is a Ga-rich reconstruction on a N-polar surface, it seems natural that the majority of the electrons reside on the nonmetallic nitrogen and the empty state tends to be localized at the outermost Ga.

Additional growth experiments by initially exposing ZrB_2 layers to either Ga flux or active nitrogen flux, and also by changing the Ga/N flux ratio, consistently produced GaN films with N polarity. This is in contrast with our previous study on direct growth of GaN on Si, where a N-rich nucleation condition was critical for monopolar film growth [11]. The experimental results suggest the existence of a stable interface structure which is less sensitive to the Ga/N flux ratio compared to the GaN(0001)-Si(111) interface and that this interface structure facilitates monopolar GaN film growth on ZrB_2.

The stability of the GaN(0001)-ZrB_2(0001) interface was studied in detail using standard density functional theory (DFT) methods based on the generalized gradient approximation (GGA) [14–16] in order to clarify the origin of the mono N polarity of the grown films. Six interface models denoted by model number m (where $m = 1$–6) with specific bonding arrangements between GaN(0001) and ZrB_2(0001), and GaN[11$\bar{2}$0] $\parallel$ ZrB_2[11$\bar{2}$0], were first constructed using bulk crystalline configurations. Models 1, 2, and 3 follow closely the three models proposed earlier in a related (1×1) GaN-ZrB_2 interface study based on continuous periodic slabs [17]. In the present work, the $(\sqrt{3} \times 1)$ basal dimensions of the all supercells were fixed at 5.489 Å $\times$ 3.169 Å (surface area $A =$ 17.40 Å^2), while the dimension perpendicular to the interface is approximately 38 Å and is chosen to minimize coupling between separated free-surface terminated slabs. Three GaN bilayers were used to represent the GaN side of the interface, while three Zr-B_2 layers were used for the ZrB_2 system. The interface and surface structures of our six models were independently optimized. For each separated or bonded configuration, the atomic coordinates were fully relaxed to their zero force positions by *ab initio* simulations [18], leading to the optimized structures shown in the six models depicted in Fig. 3.

The computed energy difference between the joined and separated optimized slabs is given by

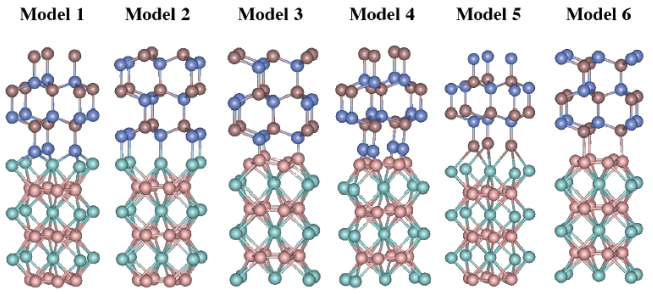

FIG. 3 (color). Atomistic representations of the six GaN(0001)-ZrB_2(0001) interface models. The atoms are represented by spheres: Ga (brown), N (dark blue), Zr (light blue), and B (pink). Models 1, 4, and 6 are N-polar, while models 2, 3, and 5 are Ga-polar.

$$\Delta E_{\text{slab}} = E_{\text{slab}}^{\text{GaN/ZrB}_2} - E_{\text{slab}}^{\text{GaN}} - E_{\text{slab}}^{\text{ZrB}_2}. \quad (1)$$

This corresponds to the energy of adhesion of isolated GaN and ZrB_2 slabs (with free surfaces) and is related to the interface energy Γ_m through the equation

$$\Gamma_m(\mu_{\text{Ga}}, \mu_{\text{Zr}}) = \Delta E_{\text{slab}}/A + \sigma^{\text{ZrB}_2}(\mu_{\text{Zr}}) + \sigma^{\text{GaN}}(\mu_{\text{Ga}}). \quad (2)$$

This approach is similar to that reported previously by Zhang and Smith [19].

The interface energy Γ, as defined by Eq. (2), is a thermodynamic function of the chemical potentials of its constituents μ_{Zr} μ_{B}, μ_{Ga}, and μ_{N}. This dependence can be further simplified by eliminating μ_{B} and μ_{N} using the thermodynamic equilibrium conditions $\mu_{\text{Zr}} + 2\mu_{\text{B}} = \mu_{\text{ZrB}_2}^{\text{bulk}}$ and $\mu_{\text{Ga}} + \mu_{\text{N}} = \mu_{\text{GaN}}^{\text{bulk}}$, leading to a Γ dependence on μ_{Ga} and μ_{Zr} only. The surface formation energy terms σ^{ZrB_2} and σ^{GaN} are linear functions of μ_{Zr} and μ_{Ga} and were calculated using seven-layer models of separate ZrB_2 and GaN cells similar to the work of Yamamoto *et al.* [20]. The value of $\mu_{\text{Ga}}(\mu_{\text{Zr}})$ spans a range from that of pure elemental Ga (Zr) taken as zero, to that of Ga (Zr) in GaN (ZrB_2); i.e., $\Delta H^f[\text{GaN}] \le \mu_{\text{Ga}} \le 0$ and $\Delta H^f[\text{ZrB}_2] \le \mu_{\text{Zr}} \le 0$, where the formation enthalpies of bulk GaN and ZrB_2 are given by

$$\Delta H^f[\text{GaN}] = \mu_{\text{GaN}}^{\text{bulk}} - \mu_{\text{Ga}}^{\text{bulk}} - \tfrac{1}{2}\mu_{N_2}^{\text{gas}} = -0.813 \text{ eV} \quad (3)$$

and

$$\Delta H^f[\text{ZrB}_2] = \mu_{\text{ZrB}_2}^{\text{bulk}} - \mu_{\text{Zr}}^{\text{bulk}} - 2\mu_B^{\text{bulk}} = -2.952 \text{ eV}. \quad (4)$$

The μ^{bulk} values were calculated as the bulk energies per formula unit, and our ΔH results compare well with previous calculated values [21,22].

Three-dimensional plots of interface energy Γ_m as a function of both μ_{Ga} and μ_{Zr} were constructed for the six models [23], and the results are summarized in Table I, listing the Γ_m values at the extreme values of the chemical potentials μ_{Ga} and μ_{Zr}. The chemical potential

TABLE I. Interface energies of the six models at the four extreme values of the allowed gallium and zirconium chemical potentials μ, showing that model 1 is preferred. The lowest interface energy Γ for each model considered is given in bold font. Chemical potentials and interface energies are given in eV and eV/Å^2, respectively.

μ_{Ga}	μ_{Zr}	Γ_1	Γ_2	Γ_3	Γ_4	Γ_5	Γ_6
−0.813	−2.952	−0.031	0.219	**0.179**	**0.052**	0.211	0.272
−0.813	0.000	**−0.201**	**0.050**	0.349	0.222	0.042	0.442
0.000	−2.952	0.016	0.266	0.226	0.099	0.164	**0.225**
0.000	0.000	−0.154	0.096	0.395	0.269	**−0.005**	0.395

$\mu_{Ga} = -0.813$ eV represents the N-rich condition, $\mu_{Ga} = 0$ the Ga-rich condition, $\mu_{Zr} = -2.952$ eV the *B*-rich condition, and $\mu_{Zr} = 0$ the Zr-rich condition. The lowest interface energy for each model is given in bold font in Table I, occurring at the chemical potentials corresponding precisely to each optimized interface shown in Fig. 3. Model 1 has the lowest overall energy of -0.201 eV/Å^2 with an interface structure consisting of tetrahedrally coordinated N, i.e., one Ga-N bond and three Zr-N bonds. In addition, over the entire chemical potential parameter space of μ_{Zr} and μ_{Ga}, i.e., within the Γ_1 column in Table I, model 1 also exhibits the widest thermodynamic stability range, becoming only slightly metastable in the Ga- and B-rich limit. This result implies that GaN grown on a Zr-terminated ZrB_2 surface is expected to be N-polar.

Thermodynamically, the only other stable interface is model 5, with $\Gamma_5 = -0.005$ eV/Å^2, while the other four models are metastable, i.e., $\Gamma_{2,3,4,6} > 0$. In the case of GaN grown on a B-terminated ZrB_2 surface, our calculations show that model 4, albeit marginally metastable with $\Gamma_4 = 0.052$ eV/Å^2, is more favorable than models 3 and 6, thus also leading to N-polar GaN. While this growth scenario is seemingly prohibited by thermodynamic considerations, it is nevertheless possible under the kinetically driven MBE process. Collectively, our results confirm the experimental observations that GaN grown directly on ZrB_2 is consistently N-polar regardless of the Ga/N flux ratio and also the termination of ZrB_2.

In summary, GaN films were grown epitaxially on Si(111) via ZrB_2 buffer layers. Ga-induced N-polar related reconstructed structures, i.e., GaN(000$\bar{1}$)-(3×3), (6×6), and $c(6 \times 12)$, were observed in atomic resolution on insulating GaN film surfaces using NC-AFM, thus establishing the N polarity of the GaN films. The interface structures were studied in detail by first-principles DFT-GGA calculations, and the results confirm the experimental observations of N-polar GaN grown by MBE on ZrB_2(0001). This study demonstrates the suitability of the ZrB_2(0001) film as an ideal buffer layer for growing monopolar and undoped GaN films on Si substrates. Atomically resolved ZrB_2(0001)-(2×2) structure was observed routinely by STM after moderate heat treatment to remove the surface oxide on the ZrB_2 buffer layers prepared *ex situ*. Such a simple cleaning procedure is easily adaptable to device fabrication processes. The uniform monopolarity achieved by this approach helps to minimize the formation of inversion domains in the GaN film, which would lead to improved performance in device structures. Coupled with metallicity of ZrB_2 serving as a reflective layer enabling efficient use of emitted light while also serving as a contact electrode, the ZrB_2 buffer layer has the promising potential for improving GaN-based optoelectronic devices.

Z. T. W. and Y. Y.-T. contributed equally to this work. This work was supported in part by the National Science Foundation Grants No. DMR-0221993 and No. DMR-0303237.

*Permanent address: Institute of Physics, Chinese Academy of Sciences, Beijing 100080, People's Republic of China.

[1] S. Nakamura *et al.*, Appl. Phys. Lett. **64**, 1687 (1994); Jpn. J. Appl. Phys. **35**, L74 (1996).
[2] See, for example, A. Krost and A. Dadgar, Phys. Status Solidi A **194**, 361 (2002), and references therein.
[3] D. E. Aspnes and A. A. Studna, Phys. Rev. B **27**, 985 (1983).
[4] E. Natali *et al.*, Jpn. J. Appl. Phys. **41**, L1140 (2002).
[5] S. Otani and Y. Ishizawa, J. Cryst. Growth **165**, 319 (1996).
[6] J. Suda and H. Matsunami, J. Cryst. Growth **237–239**, 1114 (2002); R. Liu *et al.*, Appl. Phys. Lett. **81**, 3182 (2002); S. Kamiyama *et al.*, Phys. Status Solidi A **200**, 67 (2003).
[7] C.-W. Hu *et al.*, J. Cryst. Growth **267**, 554 (2004).
[8] J. Tolle *et al.*, Appl. Phys. Lett. **82**, 2398 (2003).
[9] J. Tolle *et al.*, Appl. Phys. Lett. **84**, 3510 (2004).
[10] E. S. Hellman, MRS Internet J. Nitride Semicond. Res. **3**, 11 (1998); M. Sumiya and S. Fuke, *ibid.* **9**, 1 (2004).
[11] Z. T. Wang *et al.*, Appl. Phys. Lett. **87**, 032110 (2005).
[12] T. Aizawa *et al.*, Phys. Rev. B **65**, 024303 (2002).
[13] A. R. Smith *et al.*, Phys. Rev. Lett. **79**, 3934 (1997); Appl. Phys. A: Mater. Sci. Process. **66**, S947 (1998).
[14] We used the PW91 form of the GGA functional [15] and a plane wave pseudopotential method as implemented in the VASP code [16].
[15] J. P. Perdew *et al.*, Phys. Rev. B **46**, 6671 (1992).
[16] G. Kresse and J. Furthmüller, Phys. Rev. B **54**, 11 169 (1996); Comput. Mater. Sci. **6**, 15 (1996); G. Kresse and J. Hafner, J. Phys. Condens. Matter **6**, 8245 (1994).
[17] J. Iwata *et al.*, Appl. Phys. Lett. **83**, 2560 (2003).
[18] A $5 \times 3 \times 1$ Monkhorst-Pack *k*-point grid was used in all calculations together with a 400 eV plane wave cutoff to achieve a force accuracy of 0.01 eV/Å.
[19] W. Zhang and J. R. Smith, Phys. Rev. Lett. **85**, 3225 (2000).
[20] K. Yamamoto *et al.*, Phys. Rev. B **60**, 15 617 (1999).
[21] P. Vajeeston *et al.*, Phys. Rev. B **63**, 045115 (2001).
[22] M. Fuchs *et al.*, Phys. Rev. B **65**, 245212 (2002).
[23] P.-L. Liu *et al.*, Phys. Rev. B (to be published).